

Topological properties of multilayers and surface steps in the SnTe material class

Wojciech Brzezicki,¹ Marcin M. Wysokiński,¹ and Timo Hyart¹

¹*International Research Centre MagTop, Institute of Physics, Polish Academy of Sciences,
Aleja Lotników 32/46, PL-02668 Warsaw, Poland*

Surfaces of multilayer semiconductors typically have regions of atomically flat terraces separated by atom-high steps. Here we investigate the properties of the low-energy states appearing at the surface atomic steps in $\text{Sn}_{1-x}\text{Pb}_x\text{Te}_{1-y}\text{Se}_y$. We identify the important approximate symmetries and use them to construct relevant topological invariants. We calculate the dependence of mirror- and spin-resolved Chern numbers on the number of layers and show that the step states appear when these invariants are different on the two sides of the step. Moreover, we find that a particle-hole symmetry can protect one-dimensional Weyl points at the steps. Since the local density of states is large at the step the system is susceptible to different types of instabilities, and we consider an easy-axis magnetization as one realistic possibility. We show that magnetic domain walls support low-energy bound states because the regions with opposite magnetization are topologically distinct in the presence of non-symmorphic chiral and mirror symmetries, providing a possible explanation for the zero-bias conductance peak observed in the recent experiment [Mazur *et al.*, arXiv:1709.04000].

$\text{Sn}_{1-x}\text{Pb}_x\text{Te}_{1-y}\text{Se}_y$ multilayers have attracted interest due to experimentally observed 3D topological crystalline insulator phase [1–3] with protected surface Dirac cones [4, 5] and theoretically predicted 2D quantum spin Hall insulator [6, 7] and topological crystalline insulator [8–10] phases supporting protected edge modes. Remarkably, various defects also give rise to low-energy states in this system [11, 12]. Robust 1D modes were observed at the surface atomic steps separating regions of even and odd number of layers [12], and they can be understood as topologically protected flat bands in the case of a simplified model with a chiral symmetry [13]. In a more accurate description these step modes have a band width but the local density of states (LDOS) is large so that the system is expected to be susceptible to formation of spin, charge, orbital or superconducting order [11, 14, 15]. Indeed, recent experiments indicate that an order parameter emerges at low temperatures and surprisingly it is accompanied with an appearance of a robust zero-bias conductance peak (ZBCP) in the tunneling conductance [16, 17]. The temperature and magnetic field dependence of the energy gap are consistent with the BCS theory suggesting the existence of superconductivity and under such circumstances the ZBCP is often interpreted as an indication of Majorana modes [16–19]. The Majorana zero modes are intensively searched non-Abelian quasiparticles which hold a promise for topological quantum computation [20]. Therefore, this experimental finding calls for a critical theoretical study of the different mechanisms which may explain the appearance of the ZBCP.

In this Letter we show that $\text{Sn}_{1-x}\text{Pb}_x\text{Te}_{1-y}\text{Se}_y$ multilayers are a paradigmatic system for realization of symmetry-protected topological phases due to emergent symmetries of the low-energy theory, and therefore the ZBCP can appear without the existence of superconductivity. We first show that the important 2D bulk topological invariants are the mirror-resolved Chern number (existing due to structural mirror symmetry) and

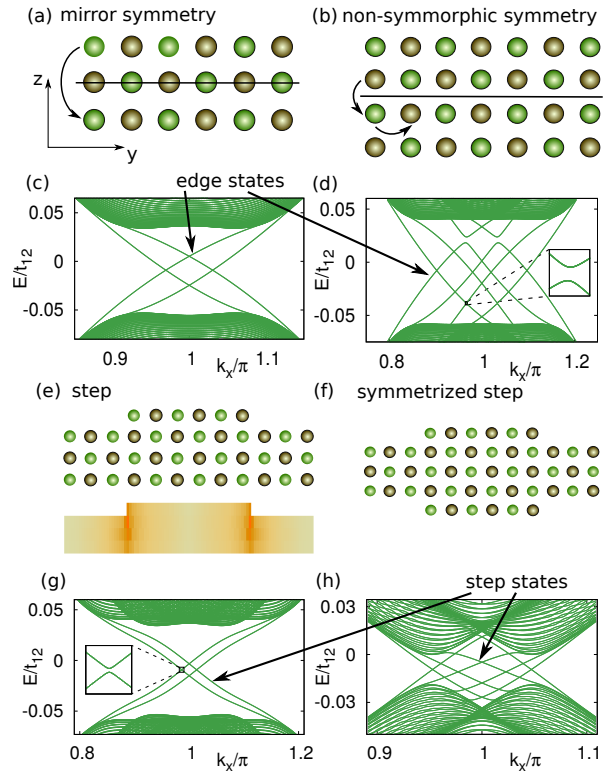


FIG. 1. (a),(b) Schematic views of the $\text{Sn}_{1-x}\text{Pb}_x\text{Te}_{1-y}\text{Se}_y$ multilayers stacked in the (001) direction. Green/grey balls are $(\text{Sn},\text{Pb})/(\text{Te},\text{Se})$ atoms. For odd (even) number of layers there exists symmorphic (non-symmorphic) mirror symmetry. (c),(d) The corresponding edge-states spectra. (e) Surface atomic steps describing an interface between three- and four-layer systems and (f) a symmetrized atomic step. (g),(h) The corresponding spectra for step modes. The panel below (e) shows local density of states of the step states. The width of the sample is $N_y = 600$.

spin-resolved Chern number (due to approximate spin-rotation symmetry). For odd number of layers the mirror symmetry is a standard point-group operation [Fig. 1(a)]

whereas for even number of layers it is a non-symmorphic (NS) symmetry [Fig. 1(b)], so that adding one layer can change the topology of the system [9, 10]. We calculate the dependence of the Chern numbers on the number of layers and show that the step states appear when these invariants are different on the two sides of the step. The theory and experiment [12, 13] attribute step states only to odd-height steps, but we predict that also even-height steps can exhibit step-states consistent with other experiment [21]. Moreover, an approximate particle-hole symmetry can protect 1D Weyl points at the steps.

We discuss the conditions under which a spontaneous symmetry breaking gives rise to an energy gap at the step and we study an easy-axis magnetic order as one possibility. We show that magnetic domain walls (DWs) support low-energy bound states because the regions with opposite magnetization are topologically distinct in the presence of NS chiral and mirror symmetries. Moreover, due to the appearance of DWs the Fermi level is pinned to the energy of the DW states for a range of electron density providing a possible explanation for the ZBCP observed in the experiment [16]. The temperature and magnetic field dependencies of the experimentally observed gap and ZBCP are consistent with our theory.

Our starting point is a p -orbital tight-binding Hamiltonian describing bulk topological crystalline insulator in $\text{Sn}_{1-x}\text{Pb}_x\text{Te}_{1-y}\text{Se}_y$ -material class [5]

$$\begin{aligned} H = & m \sum_j (-1)^j \sum_{\mathbf{r}, \alpha} \hat{c}_{j\alpha}^\dagger(\mathbf{r}) \cdot \hat{c}_{j\alpha}(\mathbf{r}) \\ & + \sum_{j, j'} t_{jj'} \sum_{\langle \mathbf{r}, \mathbf{r}' \rangle, \alpha} \hat{c}_{j\alpha}^\dagger(\mathbf{r}) \cdot \hat{d}_{\mathbf{r}\mathbf{r}'} \hat{d}_{\mathbf{r}\mathbf{r}'} \cdot \hat{c}_{j'\alpha}(\mathbf{r}') + \text{H.c.} \\ & + \sum_j i\lambda_j \sum_{\mathbf{r}, \alpha, \beta} \hat{c}_{j\alpha}^\dagger(\mathbf{r}) \times \hat{c}_{j\beta}(\mathbf{r}) \cdot \hat{\sigma}_{\alpha, \beta}, \end{aligned} \quad (1)$$

where $\hat{c}_{j\alpha}(\mathbf{r})$ are vectors of fermionic operators corresponding to p_x -, p_y - and p_z -orbitals and the indices denote the sublattice $j \in \{1, 2\}$ [(Sn,Pb)/(Te,Se) atoms], spin α and lattice site \mathbf{r} . Here $\hat{\sigma}_{\alpha, \beta}$ is a vector of Pauli matrices and $\hat{d}_{\mathbf{r}\mathbf{r}'}$ are unit vectors pointing from \mathbf{r} to \mathbf{r}' . When not otherwise stated we use $m = 1.65$ eV, nearest-neighbor (inter-sublattice) hoppings $t_{12} = 0.9$ eV, next-nearest-neighbor hoppings $t_{11} = -t_{22} = -0.5$ eV and spin-orbit couplings $\lambda_1 = \lambda_2 = \lambda = 0.3$ eV [22].

In the k -space, choosing a cubic unit cell with internal sites at the corners labeled by $i = 1, \dots, 8$ [23], the 3D bulk Hamiltonian can be represented as

$$\begin{aligned} \mathcal{H}(\mathbf{k}) = & m \mathbb{1}_2 \otimes \mathbb{1}_3 \otimes \Sigma + t_{12} \sum_{\alpha=x, y, z} \mathbb{1}_2 \otimes (\mathbb{1}_3 - L_\alpha^2) \otimes h_\alpha^{(1)}(k_\alpha) \\ & + t_{11} \sum_{\alpha \neq \beta} \mathbb{1}_2 \otimes \left(\mathbb{1}_3 - \frac{1}{2} (L_\alpha + \varepsilon_{\alpha\beta} L_\beta)^2 \right) \otimes h_{\alpha, \beta}^{(2)}(k_\alpha, k_\beta) \\ & + \sum_{\alpha=x, y, z} \lambda_\alpha \sigma_\alpha \otimes L_\alpha \otimes \mathbb{1}_8, \end{aligned} \quad (2)$$

where $\varepsilon_{\alpha\beta}$ is a Levi-Civita symbol, $L_\alpha = i\varepsilon_{\alpha\beta\gamma} L_\beta$ are the 3 ×

3 angular momentum $L = 1$ matrices, Σ is a diagonal 8×8 matrix with entries $s_i = \pm 1$ at the two sublattices, and $h_\alpha^{(1)}(k_\alpha)$ and $h_{\alpha, \beta}^{(2)}(k_\alpha, k_\beta)$ are 8×8 matrices describing hopping between the nearest-neighbor and next-nearest-neighbor lattice sites in the directions $\hat{\alpha}$ and $\hat{\alpha} + \epsilon_{\alpha\beta}\hat{\beta}$, respectively [23]. We allow the possibility to tune the spin-orbit coupling terms λ_α ($\alpha = x, y, z$) to be different from each other although in the real material $\lambda_\alpha = \lambda$.

We focus on Hamiltonian $\mathcal{H}_N(\vec{k})$ for N layers in the z -direction. The mirror symmetries with respect to the z -plane for systems with odd/even number of layers can be written as $M_z^{o/e}(k_x) = \sigma_z \otimes (2L_z^2 - 1) \otimes m_z^{o/e}(k_x)$, where m_z^o is a (momentum-independent) point-group reflection and $m_z^e(k_x)$ is a (momentum-dependent) NS operation consisting of reflection and a shift by a half lattice vector [Figs. 1(a,b)]. To calculate mirror-resolved Chern numbers C_\pm we split $\mathcal{H}_N(\vec{k})$ into two blocks in the $M_z^{o/e}(k_x)$ eigenspace. Since $M_z^{o/e}(k_x)$ anticommutes with time-reversal symmetry (TRS) operator $\mathcal{T} = \mathcal{K}\sigma_y \otimes \mathbb{1}_3 \otimes \mathbb{1}_8$, these blocks are TRS partners carrying opposite Chern numbers C_\pm [24]. We find that $C_+ = 2(-1)^n$ for $N = 2n + 1$ (we exclude $N = 1$ as an exceptional case) and $C_\pm = 0$ for $N = 2n$ ($n \in \mathbb{N}$) [25]. The edge state spectra for $N = 3$ and $N = 4$ is shown in Figs. 1(c,d). As predicted by $C_\pm = \mp 2$ we see two pairs of counter-propagating gapless edge modes in the case $N = 3$, but surprisingly we find four pairs of edge modes in a system of $N = 4$ layers. A careful examination of the spectrum in the case $N = 4$ shows that there exists small gaps (which do not vanish in the limit of large systems), so that these edge modes are consistent with $C_\pm = 0$.

To understand the existence of almost gapless edge modes in the case of $N = 4$ we notice that the momentum in the z -direction is quantized and the low-energy degrees of freedom are associated with a motion within the (x, y) -plane [26]. Therefore, the components of the spin-orbit coupling λ_α ($\alpha = x, y, z$) do not have equally strong effects on the spectrum, and the dominant contribution comes from $\lambda_z \sigma_z L_z$. Hence, turning off λ_x and λ_y is a good approximation [cf. Figs. 1(d) and 2(b)] and this leads to a spin rotation symmetry with respect to the z -axis. This symmetry allows to block-diagonalize $\mathcal{H}_N(\vec{k})$, allowing a calculation of spin-resolved Chern numbers $C_\uparrow = -C_\downarrow$ as a function of N . The results are shown in Fig. 2(a) and suggest that C_\uparrow grows linearly with N and takes values $C_\uparrow = 2 + 4m$ ($m \in \mathbb{Z}$) for odd N and $C_\uparrow = 4m$ ($m \in \mathbb{Z}$) for even N . In particular, the result for $N = 4$ is consistent with number of edge modes in Figs. 1(d), 2(b). By switching off λ_x and λ_y the spin-rotation symmetry becomes exact so that the tiny gaps originally present in the spectrum vanish completely.

These Chern numbers provide an interpretation for the appearance of the step modes. Namely, due to the bulk-boundary correspondence the step modes appear whenever C_\uparrow is different on the two sides of the step [Figs. 1(e)-

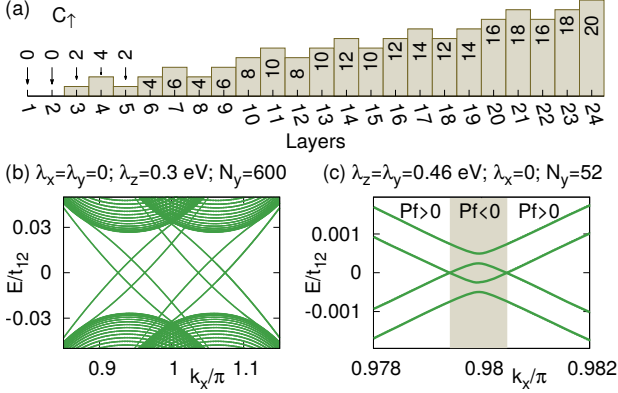


FIG. 2. (a) Spin-resolved Chern numbers C_{\uparrow} for different number of layers in a case where $\lambda_x = \lambda_y = 0$. Because we have switched off λ_x and λ_y the effective spin-orbit coupling becomes smaller. This typically does not change the mirror-resolved Chern numbers so that we can use $\lambda_z = 0.3$ eV. However, in the case of three layers the mirror-resolved Chern number was modified due to this effect, and therefore in that case we use renormalized $\lambda_z = 0.5$ eV. (b) The spectrum for a four-layer system with gapless edge modes. (c) Gapless spectrum for a step between three- and four-layer systems can be protected by a \mathbb{Z}_2 invariant if $\lambda_x = 0$.

(h)]. In the case of a step separating even and odd number of layers $\Delta C_{\uparrow} = 2+4m$ ($m \in \mathbb{Z}$) and therefore at least two pairs of helical step modes [27] always exist at these steps in agreement with Refs. [12, 13] [see Fig 1(e),(g)]. These step modes are weakly gapped because the spin-rotation symmetry is only present as an approximate symmetry. However, we can use C_{\pm} to show that these gaps vanish in the limit $N \rightarrow \infty$. Namely, by using a symmetrized step-construction shown in Fig. 1(f),(h), we find that in a system containing steps on both surfaces there exists $|\Delta C_{\pm}| = 4$ pairs of counterpropagating gapless edge modes (two pairs per surface step) protected by the mirror symmetry. In the limit $N \rightarrow \infty$ the step modes at the different surfaces are completely decoupled, and therefore a single step appearing at one of the surfaces must also support two pairs of counterpropagating gapless edge modes. Numerically, we find that the gaps indeed approach zero with increasing number of layers. Interestingly, we find that also even-height steps can exhibit $|\Delta C_{\uparrow}| = 4|m|$ ($m \in \mathbb{Z}$) pairs of step modes consistent with the experiment [21], but the appearance of these step modes depends on N on each side of the step as described by the corresponding values of C_{\uparrow} .

In the case of a one atom-high step and finite N the step modes are weakly gapped even though C_{\pm} are different on two sides of the step because the mirror symmetry $M_z(k_x)$ is symmorphic (NS) on the side with odd N (even N) so that the step breaks the mirror symmetry and hybridizes the mirror blocks. However, we find that the step modes can still be exactly gapless as long as $\lambda_x = 0$ [Fig. 2(c)]. This effect comes from the existence of an

effective particle-hole symmetry which together with a mirror symmetry gives rise to an antiunitary chiral symmetry $\mathcal{S} = \mathcal{K}\sigma_y \otimes (2L_x^2 - 1) \otimes (i\Sigma m_x)$, where m_x is a mirror reflection with respect to the x -plane interchanging the sublattices [23]. Due to this symmetry the Hamiltonian for a system with finite width N_y in y -direction $\mathcal{H}_{N_y}(k_x)$ supports a \mathbb{Z}_2 Pfaffian-invariant, which protects a 1D Weyl point if it changes sign as a function of k_x [28, 29]. As demonstrated in Fig. 2(c) this kind Weyl points can be realized at the steps if $\lambda_x = 0$, so that even in finite systems the step modes can be almost gapless.

Since we have now established the topological origin of the gapless step modes in the non-interacting system, we turn our attention to the correlation effects (e.g. spin, charge, orbital or superconducting order), which are inevitably present due to the large LDOS [11, 14, 15]. Here our aim is to demonstrate that there exists also a mechanism for the appearance of the ZBCP in the absence of superconductivity without performing a detailed analysis of the competition between different types of order. We require that the order parameter must open an energy gap, which means that it must break the approximate symmetries allowing the definition of the topological invariants $C_{\uparrow(\downarrow)}$ and C_{\pm} . Thus, for concreteness we assume that there exists a magnetic instability in the vicinity of the steps (either due to magnetic impurities or the electrons in vicinity of steps) giving rise to a Zeeman field

$$H_Z = \sum_j \sum_{\mathbf{r}, \alpha, \beta} \mathbf{h} \cdot \hat{\sigma}_{\alpha, \beta} \hat{c}_{j\alpha}^{\dagger}(\mathbf{r}) \hat{c}_{j\beta}(\mathbf{r}), \quad (3)$$

Because the step modes are approximately spin-polarized along the z -direction the directions of \mathbf{h} within the (x, y) -plane are efficient in opening an energy gap, and due to spin-orbit coupling terms the magnitude of the gap depends also on the direction of \mathbf{h} within the (x, y) -plane [23]. Therefore, the system realizes an easy-axis ferromagnet and the topological defects in such kind of a system are DWs [30]. In the following we consider $\mathbf{h} = (h_x, 0, 0)$ pointing along x -direction.

To study the possibility of the existence of topologically protected DW states we need to determine the low-energy theory for a single step, the emergent symmetries and the corresponding topological invariants. Although h_x breaks TRS the spectrum of a system with two steps still exhibits Kramers degeneracy at $k_x = \pi$ [Fig. 1(g)] due to a remaining NS TRS $\mathcal{T}'(k_x) = \mathcal{K}\mathbb{1}_2 \otimes (2L_y^2 - 1) \otimes g(k_x)r_z$, where $g(k_x)$ describes a mirror reflection within the unit cell with respect to x -plane with suitable phase-factors $e^{\pm i k_x/2}$ and r_z denotes π -rotation with respect to z axis [23]. $\mathcal{T}'(k_x)$ has an interesting property that it squares to $+1$ (-1) at $k_x = 0$ ($k_x = \pi$) which yields Kramer degeneracy only at $k_x = \pi$. From each Kramers doublet at $k_x = \pi$ we can select the state with larger projection on each step, and this way we can assign half of the states to each step. Our low-energy theory is obtained by expanding the Hamiltonian around $k_x = \pi$ in

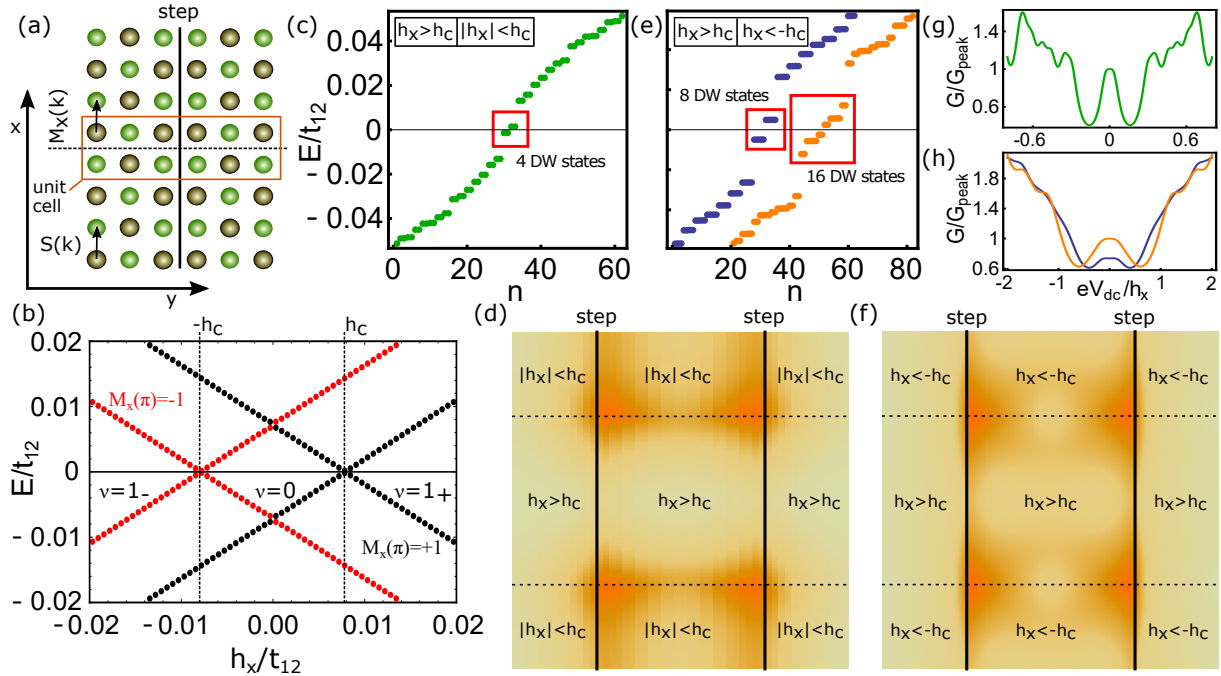


FIG. 3. (a) Schematic representation of NS symmetries $M_x(k)$ and $S(k)$ operating at a single step and containing a shift by half a lattice vector. (b) The energies of the step states at $k_x = \pi$ as a function of h_x for $N_y = 52$ and $\lambda_z = \lambda_x = 0.5$ eV. The states are coloured according to the eigenvalues of $M_x(\pi)$. There exists three topologically distinct phases denoted as trivial phase and non-trivial phases with $\nu = 1_{\pm}$. The non-trivial phases are distinct from the trivial phase due to NS chiral \mathbb{Z}_2 invariant ν [23, 31]. The lower index ± 1 describes the subspace of $M_x(\pi) = \pm 1$ where the band-inversion occurs. (c),(d) Spectrum and LDOS for a system with DWs separating trivial and non-trivial phases. The system supports 4 low-energy bound states at the 4 DWs. The parameters are $N_x = 260$, $N_y = 52$ and $\lambda_z = \lambda_x = 0.5$ eV. In the trivial (non-trivial) phase $h_x = 0.003$ eV ($h_x = 0.04$ eV). (e), (f) Spectrum and LDOS for a system with DWs separating two non-trivial phases with opposite magnetizations. The system supports 8 low-energy bound states at the 4 DWs [blue dots in (e) and (f)]. If the number of DWs is increased to 8 there exists 16 low-energy bound states [orange dots in (e)]. The parameters are $N_x = 160$, $N_y = 140$, $|h_x| = 0.034$ eV, $\lambda_z = 0.5$ eV and $\lambda_x = 0$. (g),(h) The differential conductance G as a function of bias voltage V_{dc} [23] corresponding to spectra in (c) and (e), respectively.

one of the subspaces of the projected states. By assuming $\lambda_y = 0$ we notice that the system supports a NS mirror symmetry $M_x(k_x) = \sigma_x \otimes (2L_x^2 - 1) \otimes g(k_x)$ and NS chiral symmetry $S(k_x) = i\sigma_y \otimes \mathbb{1}_3 \otimes \sum m_x g(k_x)$ [Fig. 3(a)].

We find that in the presence of these symmetries there exists three topologically distinct phases shown in Fig. 3(b). The trivial phase for $|h_x| < h_c$ is separated from the two non-trivial ones by the energy gap closings at $h_x = \pm h_c$. The non-trivial phases are characterized by a NS chiral \mathbb{Z}_2 invariant $\nu = 1$ [23, 31]. Moreover, the phases at $h_x < -h_c$ and $h_x > h_c$ are topologically distinct because the band-inversions when going from trivial phase to non-trivial ones occur in the different subspaces of the mirror eigenvalues $M_x(\pi) = \pm 1$. It is not a priori known whether the DWs between the topologically distinct phases in this symmetry class support DW states [31]. However, numerically we find that the interface between a trivial phase and a non-trivial one yields one low-energy bound state per DW, whereas the interface between two non-trivial phases with opposite h_x gives rise to two low-energy bound states per DW [Figs. 3(c)-

f)]. The number of low-energy bound states in each case is consistent with the number of zero-energy DW states expected in the case of smooth DWs [23]. Although these states resemble the zero-energy DW states considered in the context of Dirac equation [32] and Su-Schrieffer-Heeger (SSH) model [33–35], there is an important difference coming from the fact that they are realized in a model belonging to a different symmetry class. Namely, the appearance of the DW breaks the NS symmetries, and therefore the energies of these states are not exactly zero even in the limit of large systems [23]. Moreover, the energies depend on the tight binding parameters and in this sense they resemble the topological DW states in systems with more complicated unit cells consisting of three or more atoms [36]. Nevertheless, we find that for realistic system parameters the DW states appear close to the zero energy [23].

Because the DW states are not exactly at zero energy, one would expect that in high-resolution tunneling spectroscopy it would be possible to observe two splitted peaks in the tunneling conductance in the vicinity of zero

voltage. However, already quite small broadening of the energy levels leads to a single ZBCP [Fig. 3(g), (h)] [23]. Moreover, we point out that for sufficiently large density of DWs the DW bound states will hybridize and form a continuous impurity band inside the energy gap leading to a single ZBCP where the height of the peak depends on the density of DWs [Fig. 3(g), (h)]. The ZBCP is robust against variations of the density because in analogy to the SSH model [35] we expect that the DWs are the lowest energy charged excitations in the system, and therefore small density of excess electrons (or excess holes) is accommodated in the system by increasing the number of DWs, so that up to some critical variation of the density the Fermi level is pinned to the energy of the DW states. Similar situation occurs in quantum Hall ferromagnets where the lowest energy charged excitations are topological spin textures called skyrmions [37] which appear due to excess electrons and have been observed using NMR techniques [38]. We point out that also the theoretically expected parameteric dependencies of the ZBCP and the energy gap are consistent with the experimental observations [16]. The increase of temperature will lead to a suppression of the order parameter decreasing the energy gap. The external magnetic field leads to a confinement between the DWs similarly as a symmetry breaking term in the SSH model [35], so that the number of DWs and the magnitude of the ZBCP decrease. Furthermore, we find that by increasing the Zeeman field the energy gap of the system decreases and the system undergoes a transition to gapless phase [23]. Therefore, all the experimental observations can be explained without requiring the existence of superconductivity.

We thank T. Dietl, J. Tworzydlo, L. Skowronek, G. Mazur and M. Cuoco for discussions. The work is supported by the Foundation for Polish Science through the IRA Programme co-financed by EU within SG OP Programme. W.B. also acknowledges support by Narodowe Centrum Nauki (NCN, National Science Centre, Poland) Project No. 2016/23/B/ST3/00839.

- [1] P. Dziawa, B. J. Kowalski, K. Dybko, R. Buczek, A. Szczerbakow, M. Szot, E. Lusakowska, T. Balasubramanian, B. M. Wojek, M. H. Berntsen, O. Tjernberg, and T. Story, “Topological crystalline insulator states in $\text{Pb}_{1-x}\text{Sn}_x\text{Se}$,” *Nature Materials* **11**, 1023 (2012).
- [2] Y. Tanaka, Zhi Ren, T. Sato, K. Nakayama, S. Souma, T. Takahashi, Kouji Segawa, and Yoichi Ando, “Experimental realization of a topological crystalline insulator in SnTe,” *Nature Physics* **8**, 800 (2012).
- [3] Su-Yang Xu, Chang Liu, N. Alidoust, M. Neupane, D. Qian, I. Belopolski, J.D. Denlinger, Y.J. Wang, H. Lin, L.A. Wray, G. Landolt, B. Slomski, J.H. Dil, A. Marcinkova, E. Morosan, Q. Gibson, R. Sankar, F.C. Chou, R.J. Cava, A. Bansil, and M.Z. Hasan, “Observation of a topological crystalline insulator phase and topo-

- logical phase transition in $\text{Pb}_{1-x}\text{Sn}_x\text{Te}$,” *Nature Communications* **3**, 1192 (2012).
- [4] Liang Fu, “Topological crystalline insulators,” *Phys. Rev. Lett.* **106**, 106802 (2011).
- [5] Timothy H. Hsieh, Hsin Lin, Junwei Liu, Wenhui Duan, Arun Bansil, and Liang Fu, “Topological crystalline insulators in the SnTe material class,” *Nature Communications* **3**, 982 (2012).
- [6] Junwei Liu and Liang Fu, “Electrically tunable quantum spin Hall state in topological crystalline insulator thin films,” *Phys. Rev. B* **91**, 081407 (2015).
- [7] S. Safaei, M. Galicka, P. Kacman, and R. Buczek, “Quantum spin Hall effect in IV-VI topological crystalline insulators,” *New J. Phys.* **17**, 063041 (2015).
- [8] Junwei Liu, Timothy H. Hsieh, Peng Wei, Wenhui Duan, Jagadeesh Moodera, and Liang Fu, “Spin-filtered edge states with an electrically tunable gap in a two-dimensional topological crystalline insulator,” *Nature Materials* **13**, 178 (2014).
- [9] Daniely Bassanezi, Ernesto Osvaldo Wrasse, and Tome M Schmidt, “Symmetry-dependent topological phase transitions in PbTe layers,” *Materials Research Express* **5**, 015051 (2018).
- [10] Augusto L. Araújo, Gerson J. Ferreira, and Tome M. Schmidt, “Suppressed topological phase transitions due to nonsymmorphism in SnTe stacking,” *Scientific Reports* **8**, 9452 (2018).
- [11] Evelyn Tang and Liang Fu, “Strain-induced partially flat band, helical snake states and interface superconductivity in topological crystalline insulators,” *Nature Physics* **10**, 964 (2014).
- [12] Paolo Sessi, Domenico Di Sante, Andrzej Szczerbakow, Florian Glott, Stefan Wilfert, Henrik Schmidt, Thomas Bathon, Piotr Dziawa, Martin Greiter, Titus Neupert, Giorgio Sangiovanni, Tomasz Story, Ronny Thomale, and Matthias Bode, “Robust spin-polarized midgap states at step edges of topological crystalline insulators,” *Science* **354**, 1269–1273 (2016).
- [13] R. Rechciński and R. Buczek, “Topological states on uneven (Pb,Sn)Se (001) surfaces,” *arXiv:1808.07779*.
- [14] G. E. Volovik, “Graphite, graphene, and the flat band superconductivity,” *JETP Letters* **107**, 516–517 (2018).
- [15] Risto Ojajärvi, Timo Hyart, Mihail A. Silaev, and Tero T. Heikkilä, “Competition of electron-phonon mediated superconductivity and Stoner magnetism on a flat band,” *Phys. Rev. B* **98**, 054515 (2018).
- [16] G.P. Mazur, K. Dybko, A. Szczerbakow, M. Zgirski, E. Lusakowska, S. Kret, J. Korczak, T. Story, M. Sawicki, and T. Dietl, “Majorana-like excitations in a ferromagnetic topological crystalline insulator,” *arXiv:1709.04000*.
- [17] Shekhar Das, Leena Aggarwal, Subhajit Roychowdhury, Mohammad Aslam, Sirshendu Gayen, Kanishka Biswas, and Goutam Sheet, “Unexpected superconductivity at nanoscale junctions made on the topological crystalline insulator $\text{Pb}_{0.6}\text{Sn}_{0.4}\text{Te}$,” *Appl. Phys. Lett.* **109**, 132601 (2016).
- [18] He Wang, Huichao Wang, Haiwen Liu, Hong Lu, Wuhao Yang, Shuang Jia, Xiong-jun Liu, XC Xie, Jian Wei, and Jian Wang, “Observation of superconductivity induced by a point contact on 3D Dirac semimetal Cd_3As_2 crystals,” *Nat. Mater.* **15**, 38 (2016).
- [19] L. Aggarwal, A. Gaurav, G. S. Thakur, Z. Haque, A. K. Ganguli, and G. Sheet, “Unconventional superconductivity at mesoscopic point contacts on the 3D Dirac

semimetal Cd_3As_2 ,” *Nat. Mater.* **15**, 32–37 (2016).

[20] R. M. Lutchyn, E. P. A. M. Bakkers, L. P. Kouwenhoven, P. Krogstrup, C. M. Marcus, and Y. Oreg, “Majorana zero modes in superconductor–semiconductor heterostructures,” *Nature Reviews Materials* **3**, 52–68 (2018).

[21] D. Iaia, C. Y. Wang, Y. Maximenko, D. Walkup, R. Sankar, F. Chou, Y. M. Lu, and V. Madhavan, “Topological nature of step edge states on the surface of topological crystalline insulator $\text{Pb}_{0.7}\text{Sn}_{0.3}\text{Se}$,” arXiv:1809.10689.

[22] For small systems the tight-binding parameters can deviate significantly from the bulk values and lead to different topological properties [10]. However, we consider small systems only for illustration purposes. Our results are based on symmetry and topological considerations which are valid for sufficiently large systems ($\gtrsim 10$ layers) where the bulk values of the parameters can be used.

[23] See Supplementary Material for more details.

[24] Ching-Kai Chiu, Jeffrey C. Y. Teo, Andreas P. Schnyder, and Shinsei Ryu, “Classification of topological quantum matter with symmetries,” *Rev. Mod. Phys.* **88**, 035005 (2016).

[25] For $N = 2n$ the $M_z^e(k_x)$ eigenspace depends on $k_x/2$. Thus the Hamiltonian blocks become 4π -periodic in k_x and they have additional TRS with respect to the point $\vec{k}^* = (2\pi, 0)$, so that $C_{\pm} = 0$.

[26] Notice that this reasoning is valid also if the states are localized in the vicinity of the surface in the z -direction even if the system itself is infinite.

[27] Due to bulk-boundary correspondence there will be $|\Delta C_{\uparrow}|$ step modes with spin \uparrow propagating in one direction and $|\Delta C_{\downarrow}| = |\Delta C_{\uparrow}|$ step modes with spin \downarrow propagating in the opposite direction.

[28] Y. X. Zhao, Andreas P. Schnyder, and Z. D. Wang, “Unified theory of PT and CP invariant topological metals and nodal superconductors,” *Phys. Rev. Lett.* **116**, 156402 (2016).

[29] Wojciech Brzezicki and Mario Cuoco, “Topological gapless phases in nonsymmorphic antiferromagnets,” *Phys. Rev. B* **95**, 155108 (2017).

[30] Also other types of order parameters can naturally support the appearance of domain walls, and the magnetic order is considered here only as an example.

[31] Ken Shiozaki, Masatoshi Sato, and Kiyonori Gomi, “ Z_2 topology in nonsymmorphic crystalline insulators: Möbius twist in surface states,” *Phys. Rev. B* **91**, 155120 (2015).

[32] R. Jackiw and C. Rebbi, “Solitons with fermion number $1/2$,” *Phys. Rev. D* **13**, 3398–3409 (1976).

[33] W. P. Su, J. R. Schrieffer, and A. J. Heeger, “Solitons in polyacetylene,” *Phys. Rev. Lett.* **42**, 1698–1701 (1979).

[34] W. P. Su, J. R. Schrieffer, and A. J. Heeger, “Soliton excitations in polyacetylene,” *Phys. Rev. B* **22**, 2099–2111 (1980).

[35] A. J. Heeger, S. Kivelson, J. R. Schrieffer, and W. P. Su, “Solitons in conducting polymers,” *Rev. Mod. Phys.* **60**, 781–850 (1988).

[36] M. Nurul Huda, S. Kezilebieke, T. Ojanen, R. Drost, and P. Liljeroth, “Tunable topological domain wall states in engineered atomic chains,” ArXiv e-prints (2018), arXiv:1806.08614 [cond-mat.mes-hall].

[37] S. M. Girvin, “The Quantum Hall Effect: Novel Excitations and Broken Symmetries,” in *Topological Aspects of Low Dimensional Systems*, edited by A. Comtet, T. Jolicoeur, S. Ouvry, and F. David (1999) cond-mat/9907002.

[38] S. E. Barrett, G. Dabbagh, L. N. Pfeiffer, K. W. West, and R. Tycko, “Optically pumped NMR evidence for finite-size skyrmions in GaAs quantum wells near Landau level filling $\nu = 1$,” *Phys. Rev. Lett.* **74**, 5112–5115 (1995).

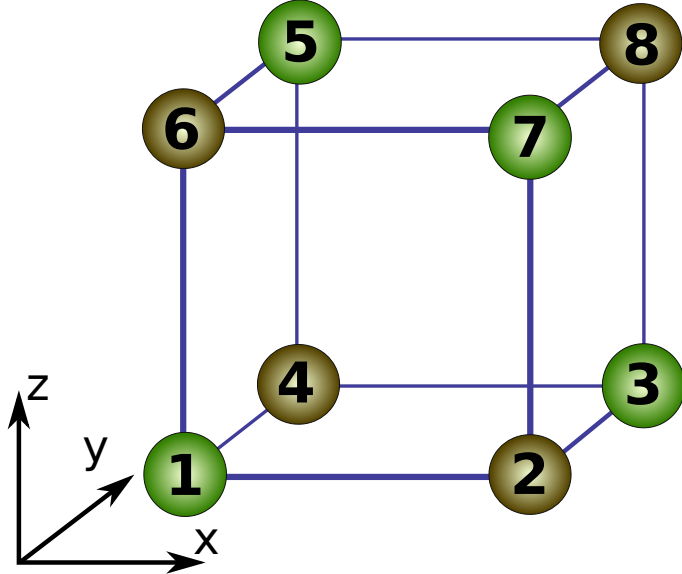


FIG. 1. The unit cell. The odd end even sites are inequivalent due to opposite mass.

SUPPLEMENTARY MATERIAL FOR "TOPOLOGICAL PROPERTIES OF MULTILAYERS AND SURFACE STEPS IN THE SNTE MATERIAL CLASS".

UNIT CELL, HAMILTONIAN AND SYMMETRIES

As discussed in the main text the 3D bulk Hamiltonian can be represented as

$$\begin{aligned} \mathcal{H}(\mathbf{k}) = & m \mathbb{1}_2 \otimes \mathbb{1}_3 \otimes \Sigma + t_{12} \sum_{\alpha=x,y,z} \mathbb{1}_2 \otimes (\mathbb{1}_3 - L_\alpha^2) \otimes h_\alpha^{(1)}(k_\alpha) + t_{11} \sum_{\alpha \neq \beta} \mathbb{1}_2 \otimes \left(\mathbb{1}_3 - \frac{1}{2} (L_\alpha + \varepsilon_{\alpha\beta} L_\beta)^2 \right) \otimes h_{\alpha,\beta}^{(2)}(k_\alpha, k_\beta) \\ & + \sum_{\alpha=x,y,z} \lambda_\alpha \sigma_\alpha \otimes L_\alpha \otimes \mathbb{1}_8, \end{aligned} \quad (1)$$

where $\varepsilon_{\alpha\beta}$ is a Levi-Civita symbol, $L_\alpha = i\varepsilon_{\alpha\beta\gamma}$ are the 3×3 angular momentum $L = 1$ matrices and $h_\alpha^{(1)}(k_\alpha)$, $h_{\alpha,\beta}^{(2)}(k_\alpha, (k_\beta))$ are matrices describing hopping between sites of 8-site unit cells (see 1) being either nearest or next nearest neighbors. These are given by,

$$h_x^{(1)}(k_x) = \begin{pmatrix} 0 & 1 + e^{-ik_x} & 0 & 0 & 0 & 0 & 0 & 0 \\ 1 + e^{ik_x} & 0 & 0 & 0 & 0 & 0 & 0 & 0 \\ 0 & 0 & 0 & 1 + e^{ik_x} & 0 & 0 & 0 & 0 \\ 0 & 0 & 1 + e^{-ik_x} & 0 & 0 & 0 & 0 & 0 \\ 0 & 0 & 0 & 0 & 0 & 0 & 0 & 1 + e^{-ik_x} \\ 0 & 0 & 0 & 0 & 0 & 0 & 1 + e^{-ik_x} & 0 \\ 0 & 0 & 0 & 0 & 0 & 1 + e^{ik_x} & 0 & 0 \\ 0 & 0 & 0 & 0 & 1 + e^{ik_x} & 0 & 0 & 0 \end{pmatrix},$$

$$h_z^{(1)}(k_z) = \begin{pmatrix} 0 & 0 & 0 & 0 & 0 & 1+e^{-ik_z} & 0 & 0 \\ 0 & 0 & 0 & 0 & 0 & 0 & 1+e^{-ik_z} & 0 \\ 0 & 0 & 0 & 0 & 0 & 0 & 0 & 1+e^{-ik_z} \\ 0 & 0 & 0 & 0 & 0 & 1+e^{-ik_z} & 0 & 0 \\ 0 & 0 & 0 & 1+e^{ik_z} & 0 & 0 & 0 & 0 \\ 1+e^{ik_z} & 0 & 0 & 0 & 0 & 0 & 0 & 0 \\ 0 & 1+e^{ik_z} & 0 & 0 & 0 & 0 & 0 & 0 \\ 0 & 0 & 1+e^{ik_z} & 0 & 0 & 0 & 0 & 0 \end{pmatrix},$$

$$h_{x,y}^{(2)} = \begin{pmatrix} 0 & 0 & 1+e^{-i(k_x+k_y)} & 0 & 0 & 0 & 0 & 0 \\ 0 & 0 & 0 & e^{ik_x+e^{-ik_y}} & 0 & 0 & 0 & 0 \\ 1+e^{i(k_x+k_y)} & 0 & 0 & 0 & 0 & 0 & 0 & 0 \\ 0 & e^{-ik_x+e^{ik_y}} & 0 & 0 & 0 & 0 & 0 & 0 \\ 0 & 0 & 0 & 0 & 0 & 0 & e^{-ik_x+e^{ik_y}} & 0 \\ 0 & 0 & 0 & 0 & 0 & 0 & 0 & 1+e^{-i(k_x+k_y)} \\ 0 & 0 & 0 & 0 & e^{ik_x+e^{-ik_y}} & 0 & 0 & 0 \\ 0 & 0 & 0 & 0 & 0 & 1+e^{i(k_x+k_y)} & 0 & 0 \end{pmatrix},$$

$$h_{y,x}^{(2)} = \begin{pmatrix} 0 & 0 & e^{-ik_x+e^{-ik_y}} & 0 & 0 & 0 & 0 & 0 \\ 0 & 0 & 0 & 1+e^{i(k_x-k_y)} & 0 & 0 & 0 & 0 \\ e^{ik_x+e^{ik_y}} & 0 & 0 & 0 & 0 & 0 & 0 & 0 \\ 0 & 1+e^{i(k_y-k_x)} & 0 & 0 & 0 & 0 & 0 & 0 \\ 0 & 0 & 0 & 0 & 0 & 0 & 1+e^{i(k_y-k_x)} & 0 \\ 0 & 0 & 0 & 0 & 0 & 0 & 0 & e^{-ik_x+e^{-ik_y}} \\ 0 & 0 & 0 & 0 & 1+e^{i(k_x-k_y)} & 0 & 0 & 0 \\ 0 & 0 & 0 & 0 & 0 & e^{ik_x+e^{ik_y}} & 0 & 0 \end{pmatrix},$$

$$h_{y,z}^{(2)} = \begin{pmatrix} 0 & 0 & 0 & 0 & 1+e^{-i(k_y+k_z)} & 0 & 0 & 0 \\ 0 & 0 & 0 & 0 & 0 & 0 & 0 & 1+e^{-i(k_y+k_z)} \\ 0 & 0 & 0 & 0 & 0 & 0 & e^{ik_y+e^{-ik_z}} & 0 \\ 0 & 0 & 0 & 0 & 0 & 0 & 0 & 0 \\ 1+e^{i(k_y+k_z)} & 0 & 0 & 0 & 0 & 0 & 0 & 0 \\ 0 & 0 & 0 & e^{-ik_y+e^{ik_z}} & 0 & 0 & 0 & 0 \\ 0 & 0 & e^{-ik_y+e^{ik_z}} & 0 & 0 & 0 & 0 & 0 \\ 0 & 1+e^{i(k_y+k_z)} & 0 & 0 & 0 & 0 & 0 & 0 \end{pmatrix},$$

$$h_{z,y}^{(2)} = \begin{pmatrix} 0 & 0 & 0 & 0 & e^{-ik_y+e^{-ik_z}} & 0 & 0 & 0 \\ 0 & 0 & 0 & 0 & 0 & 0 & 0 & e^{-ik_y+e^{-ik_z}} \\ 0 & 0 & 0 & 0 & 0 & 0 & 1+e^{i(k_y-k_z)} & 0 \\ 0 & 0 & 0 & 0 & 0 & 0 & 0 & 0 \\ e^{ik_y+e^{ik_z}} & 0 & 0 & 0 & 0 & 0 & 0 & 0 \\ 0 & 0 & 0 & 1+e^{i(k_z-k_y)} & 0 & 0 & 0 & 0 \\ 0 & 0 & 1+e^{i(k_z-k_y)} & 0 & 0 & 0 & 0 & 0 \\ 0 & e^{ik_y+e^{ik_z}} & 0 & 0 & 0 & 0 & 0 & 0 \end{pmatrix},$$

$$h_{x,z}^{(2)} = \begin{pmatrix} 0 & 0 & 0 & 0 & 0 & 0 & 1+e^{-i(k_x+k_z)} & 0 \\ 0 & 0 & 0 & 0 & 0 & e^{ik_x+e^{-ik_z}} & 0 & 0 \\ 0 & 0 & 0 & 0 & e^{ik_x+e^{-ik_z}} & 0 & 0 & 0 \\ 0 & 0 & 0 & 0 & 0 & 0 & 0 & 1+e^{-i(k_x+k_z)} \\ 0 & 0 & e^{-ik_x+e^{ik_z}} & 0 & 0 & 0 & 0 & 0 \\ 0 & e^{-ik_x+e^{ik_z}} & 0 & 0 & 0 & 0 & 0 & 0 \\ 1+e^{i(k_x+k_z)} & 0 & 0 & 0 & 0 & 0 & 0 & 0 \\ 0 & 0 & 0 & 1+e^{i(k_x+k_z)} & 0 & 0 & 0 & 0 \end{pmatrix},$$

$$h_{z,x}^{(2)} = \begin{pmatrix} 0 & 0 & 0 & 0 & 0 & 0 & e^{-ik_x} + e^{-ik_z} & 0 \\ 0 & 0 & 0 & 0 & 0 & 1 + e^{i(k_x - k_z)} & 0 & 0 \\ 0 & 0 & 0 & 0 & 1 + e^{i(k_x - k_z)} & 0 & 0 & 0 \\ 0 & 0 & 0 & 0 & 0 & 0 & 0 & e^{-ik_x} + e^{-ik_z} \\ 0 & 0 & 1 + e^{i(k_z - k_x)} & 0 & 0 & 0 & 0 & 0 \\ 0 & 1 + e^{i(k_z - k_x)} & 0 & 0 & 0 & 0 & 0 & 0 \\ e^{ik_x} + e^{ik_z} & 0 & 0 & 0 & 0 & 0 & 0 & 0 \\ 0 & 0 & 0 & e^{ik_x} + e^{ik_z} & 0 & 0 & 0 & 0 \end{pmatrix}.$$

Σ is a diagonal matrix describing mass modulation in a unit cell and has diagonal entries $(-1, 1, -1, 1, -1, 1, -1, 1)$. In the absence of the α component of SOC the system which is translationally invariant in at least x direction has a NS chiral symmetry of the form, $S_\alpha(k_x) = i\sigma_\alpha \otimes \mathbb{1}_3 \otimes \Sigma m_x g(k_x)$ where m_x is a mirror- x reflection of the cell given by,

$$m_x = \begin{pmatrix} 0 & 1 & 0 & 0 & 0 & 0 & 0 & 0 \\ 1 & 0 & 0 & 0 & 0 & 0 & 0 & 0 \\ 0 & 0 & 0 & 1 & 0 & 0 & 0 & 0 \\ 0 & 0 & 1 & 0 & 0 & 0 & 0 & 0 \\ 0 & 0 & 0 & 0 & 0 & 0 & 1 & 0 \\ 0 & 0 & 0 & 0 & 0 & 0 & 1 & 0 \\ 0 & 0 & 0 & 0 & 0 & 1 & 0 & 0 \\ 0 & 0 & 0 & 0 & 1 & 0 & 0 & 0 \end{pmatrix},$$

and $g(k_x)$ is a diagonal gauge matrix with the entries $(e^{i\frac{k_x}{2}}, e^{-i\frac{k_x}{2}}, e^{-i\frac{k_x}{2}}, e^{i\frac{k_x}{2}}, e^{i\frac{k_x}{2}}, e^{-i\frac{k_x}{2}}, e^{-i\frac{k_x}{2}}, e^{-i\frac{k_x}{2}})$. The plane of the mirror m_x cuts the unit cell into halves and interchanges the sublattices and this is why it appears in the chiral symmetry operator. Its relation to the Hamiltonian is standard, i.e., $\{\mathcal{H}_{\vec{k}}, S_\alpha(k_x)\} = 0$ for every k -point. In the main text we always use $S(k_x) \equiv S_y(k_x)$ so the y subscript is omitted for brevity. The same gauge $g(k_x)$ matrix is used for constructing the NS x -plane mirror reflection in the k -space, i.e., $M_x(k_x) = \sigma_x \otimes (2L_x^2 - 1) \otimes g(k_x)$. It satisfies the usual relation with the Hamiltonian $M_x(k_x)\mathcal{H}_{k_x, k_y, k_z}M_x^\dagger(k_x) = \mathcal{H}_{-k_x, k_y, k_z}$. Analogically the NS z -plane mirror reflection $M_z(k_x)$ can be defined as $M_z(k_x) = \sigma_z \otimes (2L_z^2 - 1) \otimes g(-k_x)m_z$ where m_z transforms the sites in the unit cell with a matrix,

$$m_z = \begin{pmatrix} 0 & 0 & 0 & 0 & 0 & 0 & 1 & 0 \\ 0 & 0 & 0 & 0 & 0 & 1 & 0 & 0 \\ 0 & 0 & 0 & 0 & 1 & 0 & 0 & 0 \\ 0 & 0 & 0 & 0 & 0 & 0 & 0 & 1 \\ 0 & 0 & 1 & 0 & 0 & 0 & 0 & 0 \\ 0 & 1 & 0 & 0 & 0 & 0 & 0 & 0 \\ 1 & 0 & 0 & 0 & 0 & 0 & 0 & 0 \\ 0 & 0 & 0 & 1 & 0 & 0 & 0 & 0 \end{pmatrix},$$

and we get $M_z(k_x)\mathcal{H}_{k_x, k_y, k_z}M_z^\dagger(k_x) = \mathcal{H}_{k_x, k_y, -k_z}$. Finally, we can also define a symmorphic π -rotation symmetry R_z in the xy plane as $R_z = \sigma_z \otimes (2L_z^2 - 1) \otimes r_z$ where,

$$r_z = \begin{pmatrix} 0 & 0 & 1 & 0 & 0 & 0 & 0 & 0 \\ 0 & 0 & 0 & 1 & 0 & 0 & 0 & 0 \\ 1 & 0 & 0 & 0 & 0 & 0 & 0 & 0 \\ 0 & 1 & 0 & 0 & 0 & 0 & 0 & 0 \\ 0 & 0 & 0 & 0 & 0 & 0 & 1 & 0 \\ 0 & 0 & 0 & 0 & 0 & 0 & 0 & 1 \\ 0 & 0 & 0 & 0 & 1 & 0 & 0 & 0 \\ 0 & 0 & 0 & 0 & 0 & 1 & 0 & 0 \end{pmatrix},$$

whose relation with the Hamiltonian is $R_z\mathcal{H}_{k_x, k_y, k_z}R_z^\dagger = \mathcal{H}_{-k_x, -k_y, k_z}$. Now, combining R_z with $M_x(k_x)$ we can obtain a y -plane mirror reflection $M_y(k_x) = R_z M_x(k_x)$, i.e., $M_y(k_x)\mathcal{H}_{k_x, k_y, k_z}M_y(k_x)^\dagger = \mathcal{H}_{k_x, -k_y, k_z}$, and by combining R_z with $M_z(k_x)$ we get an inversion symmetry, i.e., $I(k_x) = R_z M_z(k_x)$ and $I(k_x)\mathcal{H}_{\vec{k}}I^\dagger(k_x) = \mathcal{H}_{-\vec{k}}$. It can be now combined with time-reversal symmetry, $\mathcal{T} = \mathcal{K}\sigma_y \otimes \mathbb{1}_3 \otimes \mathbb{1}_8$ where \mathcal{K} is complex conjugation, in a form of

$\mathcal{Q}(k_x) = \mathcal{T}I(k_x)$ satisfying $\mathcal{Q}(k_x)\mathcal{H}_{\vec{k}}\mathcal{Q}^{-1}(k_x) = \mathcal{H}_{\vec{k}}$. Since $\mathcal{Q}^2(k_x) = -1$ for all k_x , every band is Kramers degenerate within whole Brillouin zone (BZ).

When the system is not fully 3D but consists of a finite number N of atomic layers stacked in the z direction then one complication arises. When N is even then the supercell can be constructed by stacking cubic cells vertically and replacing exponents of k_z by hopping in the real space along z . The spatial part of the symmetry operators may become richer if they permute the layers. Especially, the M_z becomes a symmorphic symmetry in case of odd N because we have to stack $(N-1)/2$ of whole cubic cells and one half extra which makes the reflection plane coincide with the central layer of the system. This leads to the M_z^o versions of the $M_z(k_x)$ operator (with no k_x dependence) whereas for even N the $M_z^e(k_x)$ is defined with the same intracell reflection m_z accompanied by a permutation of cells that reverts their order along z direction.

In both even and odd case M_z anticommutes with \mathcal{T} and commutes with the multilayer 2D Hamiltonian, i.e., $[\mathcal{H}_N(k_x, k_y), M_z^{o,e}] = 0$, which implies that the double degeneracy of every band is resolved in the M_z invariant subspaces. It is due to the peculiarity of the NS symmetry that in the even case the M_z subspaces keep internal TRS. This can be understood in a following way described in Ref. [1]. Take the eigenvectors of $M_z^e(k_x)$ and write them in the columns of matrix $U(k_x)$. In the basis given by $U(k_x)$ matrix $M_z^e(k_x)$ has a diagonal form and Hamiltonian and TRS are denoted as

$$\tilde{\mathcal{H}}_N(k_x, k_y) = U(k_x)^\dagger \mathcal{H}_N(k_x, k_y) U(k_x), \quad \tilde{\mathcal{T}} = \mathcal{K} U(k_x)^T (\sigma_y \otimes \mathbb{1}_3 \otimes \mathbb{1}_8) U(k_x). \quad (2)$$

The Hamiltonian commutes with $M_z^e(k_x)$ so it has block-diagonal form but TRS is antidiagonal due to anticommutation with $M_z^e(k_x)$. Apparently there is no TRS inside the diagonal blocks of \mathcal{H}'_N . One can however notice that $U(k_x)$ is not 2π - but 4π -periodic due to nonsymmorphicity so one can define a non-trivial unitary matrix χ that produces the 2π shift of the bands in the $U(k_x)$ basis, i.e.,

$$\chi = U(k_x + 2\pi)^\dagger U(k_x), \quad \chi \tilde{\mathcal{H}}_N(k_x, k_y) \chi^\dagger = \tilde{\mathcal{H}}_N(k_x + 2\pi, k_y). \quad (3)$$

Now, knowing that eigensubspaces of $M_z^e(k_x)$ are interchanged after a shift of 2π it is easy to notice that χ has a purely antidiagonal structure, just like $\tilde{\mathcal{T}}$. Therefore, by combining these two operators we obtain an intra-block TRS, i.e.,

$$\tilde{\mathcal{T}}_2 = \tilde{\mathcal{T}}\chi, \quad \tilde{\mathcal{T}}_2 \tilde{\mathcal{H}}_N(k_x, k_y) \tilde{\mathcal{T}}_2^{-1} = \tilde{\mathcal{H}}_N(-k_x - 2\pi, -k_y), \quad (4)$$

which is a time-reversal with respect to the $(k_x, k_y) = (2\pi, 0)$ point. This relation is enough to guarantee that the mirror-resolved Chern numbers vanish in the case of even number of layers N . Another way of resolving the global double degeneracy is to have a spin-rotation symmetry around some axis which happens when only one component of SOC is present, i.e., having only λ_z non-zero yields a symmetry given by $S_z = \sigma_z \otimes \mathbb{1}_3 \otimes \mathbb{1}_8$. The spin subspaces do not depend on spatial symmetries so the spin-resolved Chern numbers are allowed for any N .

When a step along x is introduced in the system the dimension of the k -space is further reduced to 1D and the Hamiltonian is denoted as $\mathcal{H}_{\{N, N'\}}(k_x)$ where N and N' denote the number of layers at the either side of the step edge. Note that apart from the effective single step Hamiltonian we always considered system periodic in the y direction so that the steps come in pairs and the y -plane mirror $M_y(k_x)$ is conserved. Then in the absence of λ_x another combined antiunitary operation can be defined; a chiral symmetry $\mathcal{S} = \mathcal{T}M_x(k_x)S_x(k_x)$ being symmorphic and satisfying $\mathcal{S}^2 = +1$. It allows for transformation that makes the Hamiltonian purely imaginary. Its explicit form is $\mathcal{S} = \mathcal{K}\sigma_y \otimes (2L_x^2 - 1) \otimes (i\Sigma m_x)$ and the relation with the Hamiltonian is usual anticommutation although due to antiunitarity it does not yield two off-diagonal blocks of $\mathcal{H}_{\{N, N'\}}(k_x)$. A part of \mathcal{S} symmetry is $\mathcal{T}S_x(k_x)$ which is referred as an effective particle-hole symmetry in the main text. What is peculiar about \mathcal{S} is that it is compatible with a Zeeman field term in any direction. Finally, if we set the Zeeman field as $\mathbf{h} = (h_x, 0, 0)$ in the absence of λ_y the unitary symmetries that survive are mirror $M_x(k_x)$ and chirality $S_y(k_x) \equiv S(k_x)$. The y -plane mirror $M_y(k_x)$ is not a symmetry any more as it anticommutes with a field term but together with \mathcal{T} it form a NS time-reversal symmetry $\mathcal{T}'(k_x) = \mathcal{T}M_y(k_x)$ that can be expressed as $\mathcal{T}'(k_x) = \mathcal{K}\mathbb{1}_2 \otimes (2L_y^2 - 1) \otimes g(k_x)r_z$ and it yields a relation with Hamiltonian, $\mathcal{T}'(k_x)\mathcal{H}_{\{N, N'\}}(k_x)\mathcal{T}'^{-1}(k_x) = \mathcal{H}_{\{N, N'\}}(-k_x)$. It is another peculiarity of a NS symmetry that $\mathcal{T}'^2(0) = 1$ but $\mathcal{T}'^2(\pi) = -1$ so that the Kramers degeneracy appears only at $k_x = \pi$ [1].

DEPENDENCE OF THE STEP MODE DISPERSION ON THE NUMBER OF LAYERS

As shown in Fig. 2, for increasing number of layers N the system tends to develop Dirac cones with closing of the bulk gap that are consistent with the (001) surface of the TCI. The dispersion of the step states connecting these cones becomes more and more flat, as expected.

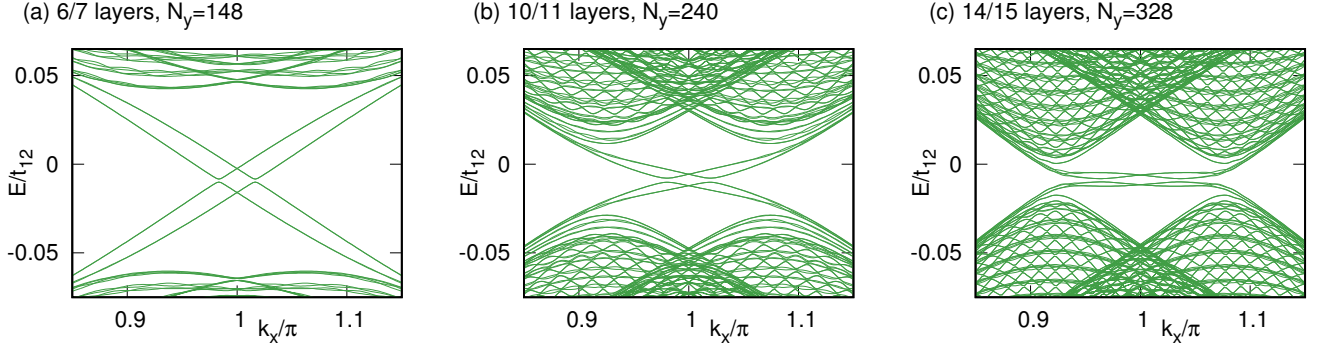


FIG. 2. Dispersion of the step modes in the case of a monoatomic step formed between (a) 6 and 7 layers, (b) 10 and 11 layers, and (c) 14 and 15 layers. N_y is the width of the sample used in each plot.

DEPENDENCE OF THE ENERGY GAP ON THE ZEEMAN FIELD

The behavior of the energy gap E_g of a system with step states is non-trivial when the Zeeman field is switched on. In Fig. 3(a) we show the dependence of E_g on h_x . Consistently with the results presented in the main text above some critical value of h_x the gap opens up to maximal value around $h_x = 0.06t_{12}$ but then it decreases and tends to close again. The dependence on the direction of the field in the xy and xz planes is shown in Figs. 3(b-c). We expect that in the case of magnetic instability there exists an easy-axis along x -direction because the magnetization in x -direction maximizes the gap and leads to a minimum of the free energy.

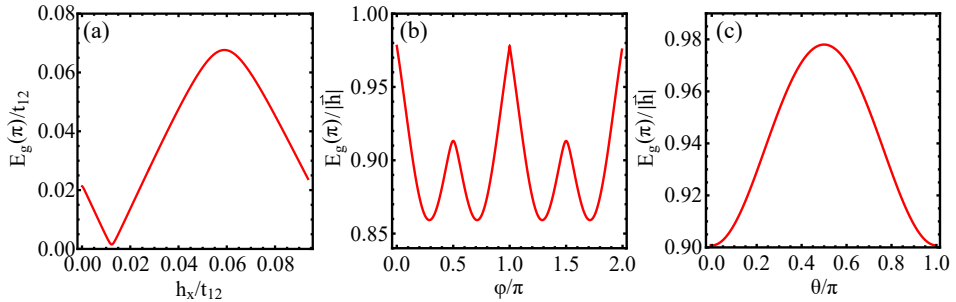


FIG. 3. (a) Dependence of the energy gap E_g at $k_x = \pi$ on the Zeeman field magnitude h_x . (b),(c) The dependence of E_g on the direction of \vec{h} within xy plane given by the azimuthal angle ϕ and xz plane given by the polar angle θ . Results are for a step formed between regions with 2 and 3 layers for $\lambda_x = \lambda_y = \lambda_z = 0.3$ eV and $N_y = 52$.

DEPENDENCE OF THE DOMAIN WALL STATE ENERGIES ON THE SYSTEM PARAMETERS

The scaling properties of the bulk gap of the step modes E_g and the energy of the DW states E_0 in case of sharp DWs are complicated and depend on the value of the Zeeman field. Here we consider the field in the x direction. In Fig. 4 we show the values of $h_x = h_x^{\max}$ that maximize the bulk gap E_g for systems of 2/3 and 6/7 layers as a function of N_y . We observe saturation of both h_x^{\max} and E_g in the limit $N_y \rightarrow \infty$. We now consider the case of optimal bulk gap and study the energies of the DW states for magnetic domains with opposite magnetization $\pm h_x$ as a function

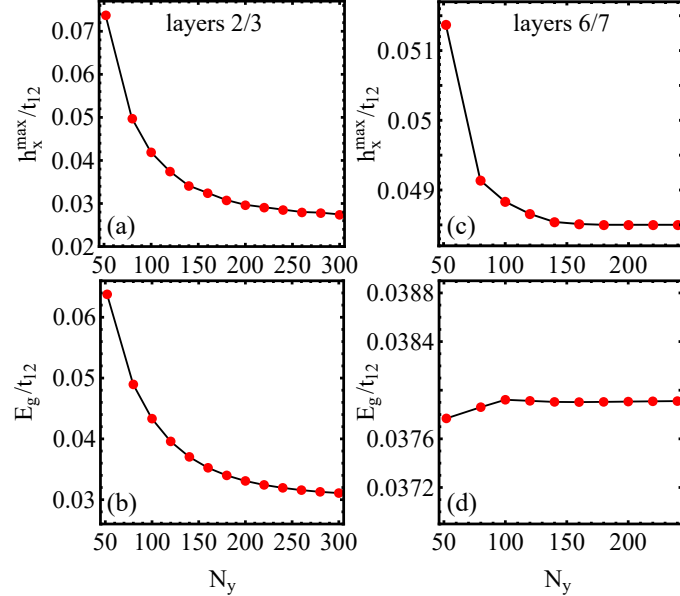


FIG. 4. Dependence of the Zeeman field h_x^{\max} maximizing the bulk gap and its maximal value E_g on N_y . ($N_y/2$ is the spacing between the two steps.) The steps are formed between regions of (a),(b) 2/3 layers and (c),(d) 6/7 layers. We have used $\lambda_z = 0.5$ eV.

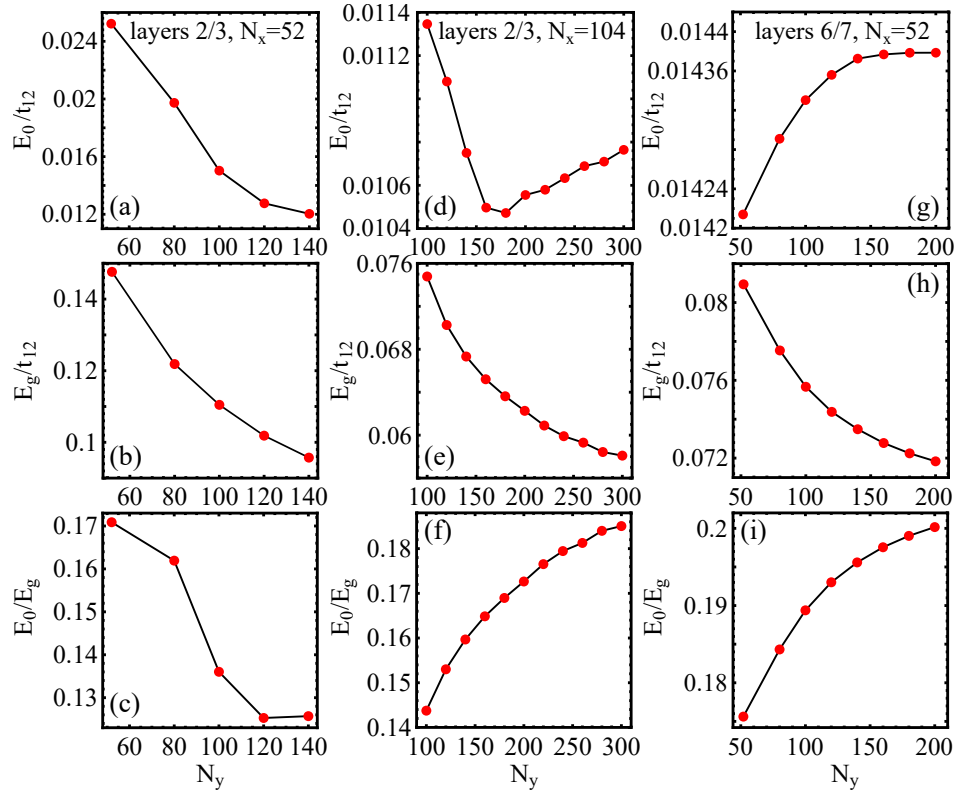


FIG. 5. Dependence of the bulk gap E_g , the energy of bound states E_0 and their ratio E_0/E_g as functions of N_y . We have chosen $h_x = h_x^{\max}$ for each N_y and considered a DW between regions with opposite magnetizations h_x and $-h_x$. The energies are shown for system sizes (a),(b),(c) 2/3 layers and $N_x = 52$, (d),(e),(f) 2/3 layers and $N_x = 104$, and (g),(h),(i) 6/7 layers and $N_x = 52$. We have used $\lambda_z = 0.5$ eV.

of the system size. The results are presented in Fig. 5 for various system sizes and we consider E_0/E_g as the figure of merit. N_y is taken in a range of roughly $N_x < N_y < 5/2N_x$. We see that E_0/E_g is typically between 0.1 and

0.2 and there is only a weak dependence on the system size. The bulk gap E_g and the energy of the DW states E_0

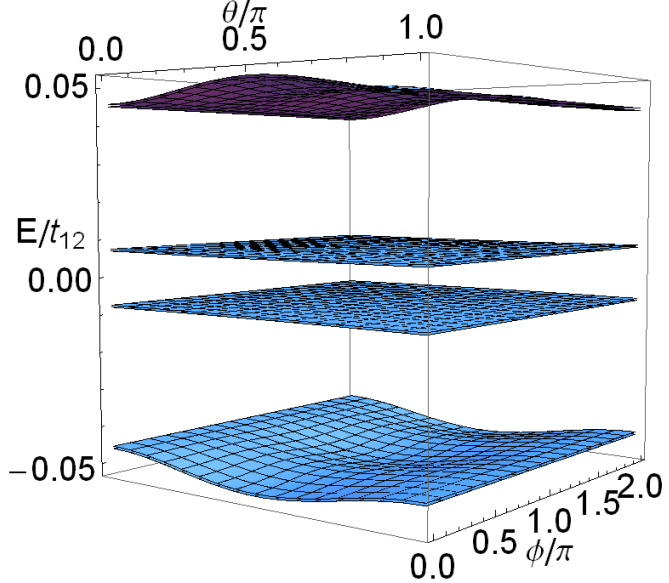


FIG. 6. Dependence of the low energy spectrum for a system with two magnetic domains with magnetization $\pm \vec{h}$ on the magnetization direction given by azimuthal ϕ and polar θ angles. The system consists of 2/3 layers with $N_x = N_y = 52$, $|h| = t_{12}/30$ and $\lambda_x = \lambda_z = 0.4$ eV.

are surprisingly immune to the changes of the Zeeman field direction. In Fig. 6 we show the low energy spectrum as function of the field direction for a fixed magnitude of the Zeeman field.

LOW-ENERGY THEORY FOR THE STEP MODES AND DOMAIN WALLS

By solving the eigenstates corresponding to one of the steps at $k_x = \pi$ and by expanding the Hamiltonian for momentum $k_x = \pi + k$, the low-energy theory for the step modes in the absence of Zeeman field can be written as

$$\mathcal{H}_{\text{step}}(k) = \Delta \sigma_0 \tau_x + v k \sigma_z \tau_0 + \tilde{v} k \sigma_0 \tau_z + \Lambda \sigma_y \tau_z + \tilde{\Lambda} k \sigma_x \tau_y, \quad (5)$$

where Δ is the energy of the step modes at $k = 0$ (in the absence of λ_x), v and \tilde{v} describe the velocities of the step modes ($|v| > |\tilde{v}|$), and Λ and $\tilde{\Lambda}$ are small terms arising due to the spin-orbit coupling λ_x . We find that in the lowest order approximation λ_y does not have any effect in the low-energy theory. If $\lambda_x = 0$ the model obeys spin-rotation symmetry around z -axis

$$S_z \mathcal{H}_{\text{step}}(k) S_z = \mathcal{H}_{\text{step}}(k), \quad S_z = \sigma_z \tau_0 \text{ for } \Lambda = \tilde{\Lambda} = 0, \quad (6)$$

and supports two pairs of gapless counterpropagating edge modes as described in the main text. Due to $\lambda_x \neq 0$ ($\Lambda \neq 0, \tilde{\Lambda} \neq 0$) the spin-rotation symmetry is weakly broken and the step modes are gapped.

Within this low-energy model the non-symmorphic symmetries become usual symmorphic symmetries, which are obtained by projecting them to the states at $k_x = \pi$. The non-symmorphic chiral symmetry defines a chiral symmetry

$$C \mathcal{H}_{\text{step}}(k) C = -\mathcal{H}_{\text{step}}(k), \quad C = \sigma_y \tau_y \quad (7)$$

and the non-symmorphic mirror symmetry leads to a relation

$$M_x \mathcal{H}_{\text{step}}(-k) M_x = \mathcal{H}_{\text{step}}(k), \quad M_x = \sigma_x \tau_x. \quad (8)$$

Additionally the system obeys time-reversal symmetry

$$\sigma_y \tau_x \mathcal{H}_{\text{step}}^*(-k) \sigma_y \tau_x = \mathcal{H}_{\text{step}}(k). \quad (9)$$

This is the most general linearized Hamiltonian in the presence of these symmetries.

The Zeeman field component h_x preserves both M_x and C , whereas h_z breaks M_x but preserves C . Therefore, we consider the effect of both of these components on the topology of the system. In the low-energy theory around $k_x = \pi$ they give rise to a Hamiltonian

$$\mathcal{H}_{\text{step}}^Z = h_z \sigma_z \tau_0 + c h_x \sigma_x \tau_0, \quad (10)$$

where the factor c takes into account the renormalization of the effect of h_x within the low-energy theory and h_z is practically unmodified due to the fact that the step modes are spin-polarized as a good approximation. Since both of these terms obey the chiral symmetry [Eq. (7)], we can utilize the chiral symmetry to block-off diagonalize the Hamiltonian

$$U^\dagger [\mathcal{H}_{\text{step}}(k) + \mathcal{H}_{\text{step}}^Z] U = \begin{pmatrix} 0 & D(k) \\ D^\dagger(k) & 0 \end{pmatrix}, \quad U = \begin{pmatrix} \tau_z & -\tau_z \\ \tau_x & \tau_x \end{pmatrix}, \quad D(k) = \begin{pmatrix} (-i\tilde{\Lambda} - v - \tilde{v})k - h_z & \Delta + ch_x - i\Lambda \\ \Delta - ch_x - i\Lambda & (-i\tilde{\Lambda} - v + \tilde{v})k - h_z \end{pmatrix}. \quad (11)$$

It is easy to see $\text{Im}\{\det[D(k)]\}$ is independent of h_x and h_z at $k = 0$ and $k \rightarrow \pm\infty$. Moreover, the sign of $\text{Im}\{\det[D(k)]\}$ is different at $k = 0$ and $k \rightarrow \pm\infty$ [see Fig. 7], and in the following we consider

$$\text{Im}\{\det[D(k \rightarrow 0)]\} > 0 \text{ and } \text{Im}\{\det[D(k \rightarrow \pm\infty)]\} < 0 \quad (12)$$

as a constraint which is always required to be satisfied. Within the low-energy theory this requirement is robustly satisfied even if we introduce an arbitrary small perturbation to the Hamiltonian. Moreover, our considerations are valid beyond the low-energy theory because if we equate the $k \rightarrow \pm\infty$ limit with $k \rightarrow 2\pi$ this constraint is always satisfied in the full theory where all the higher order terms in the expansion of $\mathcal{H}_{\text{step}}(k)$ are correctly taken into account. This follows from the fact that the chiral symmetry C originates from non-symmorphic chiral symmetry, which guarantees that a relation $\text{Im}\{\det[D(0)]\} = -\text{Im}\{\det[D(2\pi)]\}$ should always be satisfied [2]. Importantly, in the presence of the constraint (12) we can identify topologically distinct phases by plotting the trajectories of the $Z(k) = \det[D(k)]$ in the complex plane [see Fig. 7].

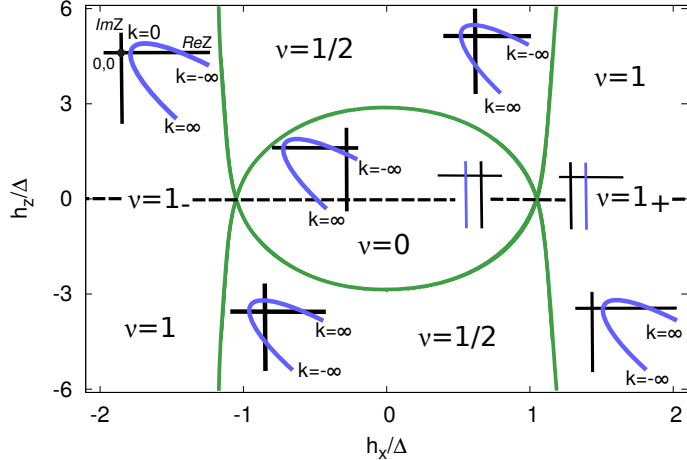


FIG. 7. Topological phase diagram of the low-energy model for the step modes as function of the Zeeman field components h_x and h_z for $\Delta = 0.003$ eV, $v = -0.114$ eV, $\tilde{v} = -0.019$ eV, $\Lambda = 0.000032$ eV, $\tilde{\Lambda} = 0.01$ eV and $c = 0.88$.

If we first set $h_z = 0$ we reproduce the phase diagram discussed in the main text. Here the non-symmorphic chiral \mathbb{Z}_2 invariant ν can be determined by plotting the trajectory of $Z(k)$ from $k = 0$ to $k = \infty$ in analogy to the trajectory plotted from $k = 0$ to $k = 2\pi$ in the case of lattice Hamiltonian obeying non-symmorphic chiral symmetry [2]. In the case of $\nu = 0$ the trajectory is on the left side of the origin and in the case $\nu = 1$ on the right side of the origin [see Fig. 7]. Therefore, these two phases cannot be smoothly deformed into each other without going through the origin (i.e. closing the energy gap). Moreover, the trajectory of $Z(k)$ from $k = -\infty$ to $k = 0$ reproduces the same trajectory so that the behavior of the Hamiltonian at the momenta $k \rightarrow \pm\infty$ can be identified with the behavior of the lattice Hamiltonian at momentum $k = 2\pi$, and therefore we expect that the full Hamiltonian where all the higher order terms in the expansion of $\mathcal{H}_{\text{step}}(k)$ are correctly taken into account would also reproduce the same behavior. Therefore, although we have identified the $\nu = 0$ and $\nu = 1$ phases using the low-energy theory we expect that

they are equivalent to the two topologically distinct phases of the full lattice Hamiltonian in this symmetry class [2]. As discussed in the main text the band-inversions at $h_x = \pm h_c$ occur at different mirror sectors so that we can additionally label the non-trivial phases as $\nu = 1_{\pm}$ as long as $h_z = 0$.

The z -component of the Zeeman field h_z breaks the mirror symmetry but preserves the chiral symmetry. Therefore for $h_z \neq 0$ the trajectories $k = 0$ to $k = \infty$ and $k = -\infty$ to $k = 0$ are no longer identical. However, as long as both of these trajectories remain on the same side of the origin, the Hamiltonians are topologically equivalent with the corresponding $\nu = 0$ (trajectory on the left side) or $\nu = 1$ (trajectory on the right side) Hamiltonians discussed above. Interestingly, in the presence of $h_z \neq 0$ there exists also a third topologically distinct phase within the low-energy theory, which we have labelled $\nu = 1/2$. In this case the trajectories from $k = -\infty$ to $k = 0$ and $k = 0$ to $k = \infty$ are on the different sides of the origin (so that in a sense half of the trajectory is on the left and half on the right). This phase does not have lattice analogue [2] but it is still a topologically distinct phase within the low-energy theory, because there necessarily exists a gap closing when deforming the Hamiltonian belonging to this topological class into a Hamiltonian belonging to either $\nu = 0$ or $\nu = 1$ topological classes in the presence of the constraint (12).

This topological phase diagram enables a full description of the properties of the magnetic DWs where the magnetization $(h_x(x), 0, h_z(x))$ varies slowly as a function of x . For such kind of smooth magnetic DWs the number of gap closings (zero energy DW states) is determined by the number of topological phase transitions occurring along the trajectory $(h_x(x), 0, h_z(x))$ as a function of x . For example if one considers a DW between $\nu = 1_+$ and $\nu = 1_-$ phases any smooth DW will lead to at least two gap closings. The low-energy theory does not allow us to calculate the DW states appearing in the case of sharp DWs where the magnetization $(h_x(x), 0, h_z(x))$ varies quickly as a function of x . However, the numerical calculations described the main text and in the supplementary material are consistent with the idea that the number of low-energy bound states appearing in the case of sharp DWs is the same as the number of gap closing points in the case of smooth DWs.

CALCULATION OF THE TUNNELING CONDUCTANCE

The tunneling current I due to applied voltage V_{dc} is described by [3]

$$I(V_{dc}) = e \int_{-\infty}^{\infty} dE T(E) [n_F(E) - n_F(E + eV_{dc})], \quad (13)$$

where n_F is Fermi function and $T(E)$ the transmission probability given by

$$T(E) = \frac{2\pi}{\hbar} \sum_{\nu, \mu} |T_{\nu\mu}|^2 A_{L\nu}(E) A_{R\mu}(E + eV_{dc}). \quad (14)$$

Here $A_{L\nu}(E)$ and $A_{R\mu}(E)$ are the spectral functions of states ν and μ localized on the left L and right R side of the tunneling barrier, and $T_{\nu\mu}$ is the tunneling matrix element. In the case of soft point-contact spectroscopy we may assume that one of the systems has a constant density of states so that

$$\frac{2\pi e}{\hbar} \sum_{\nu} |T_{\nu\mu}|^2 A_{L\nu}(E) \simeq \text{const} = I_0 \quad (15)$$

and thus in zero-temperature limit

$$G = \frac{dI}{dV} = eI_0 \sum_{\mu} A_{R\mu}(eV_{dc}). \quad (16)$$

In realistic systems the spectral functions have a broadening Γ due to electron-phonon and electron-electron interactions, disorder and coupling of the tip to the system. The simplest approximation in which these effects can be accounted for is Lorenzian form

$$A_{\mu}(E) = \frac{1}{\pi} \frac{\Gamma}{(E - \epsilon_{\mu})^2 + \Gamma^2}, \quad (17)$$

where ϵ_{μ} is the energy of state μ . This way we obtain

$$\frac{G(V_{dc})}{G_0} = \sum_{\mu} \frac{1}{(eV_{dc} - \epsilon_{\mu})^2 / \Gamma^2 + 1} \quad (18)$$

with $G_0 = eI_0/\pi\Gamma$, and this formulas has been used for plotting the tunneling conductances in the main text. Moreover, we define $G_{\text{peak}} = G(0)$ and $\Gamma_0 = \sqrt{3}E_0$, and in the main text we use $\Gamma = \Gamma_0$ in all figures. Because the DW states are not exactly at zero-energy one would observe a double-peak structure in the tunneling conductance in the case of small broadening. However, for broadening $\Gamma \geq \Gamma_0$ one observes a single zero-bias peak (see Fig. 8).

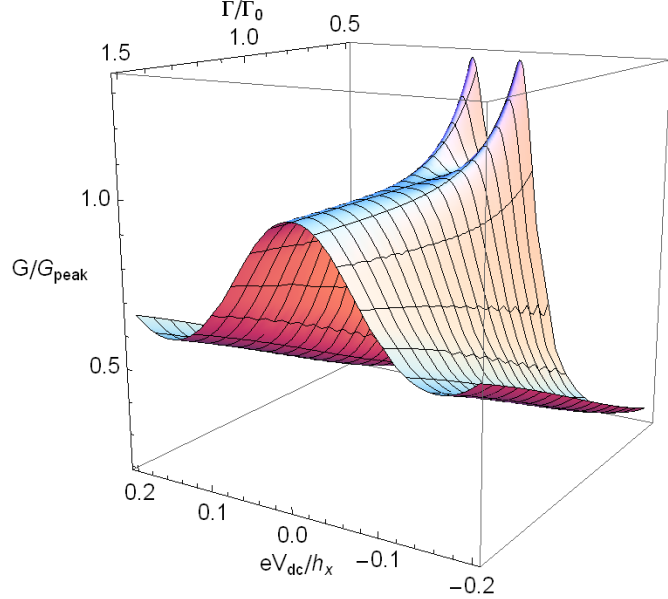


FIG. 8. Evolution from zero-bias peak to double peak structure as a function of Γ .

[1] Wojciech Brzezicki and Mario Cuoco, “Topological gapless phases in nonsymmorphic antiferromagnets,” *Phys. Rev. B* **95**, 155108 (2017).
[2] Ken Shiozaki, Masatoshi Sato, and Kiyonori Gomi, “ Z_2 topology in nonsymmorphic crystalline insulators: Möbius twist in surface states,” *Phys. Rev. B* **91**, 155120 (2015).
[3] H. Bruus and K. Flensberg, *Many-body quantum theory in condensed matter physics* (Oxford University Press, 2004).